Shadowing, binding, and off-shell effects in nuclear deep-inelastic scattering

S. A. Kulagin*

Institut für Theoretische Physik, Universität Regensburg, D-93040 Regensburg, Germany

G. Piller†

Department of Physics and Mathematical Physics, University of Adelaide, South Australia, 5005

W. Weise

Institut für Theoretische Physik, Universität Regensburg, D-93040 Regensburg, Germany

We present a unified description of nuclear deep-inelastic scattering (DIS) over the whole region $0 < x < 1$ of the Bjorken variable. Our approach is based on a relativistically covariant formalism which uses analytical properties of quark correlators. In the laboratory frame it naturally incorporates two mechanisms of DIS: (i) scattering from quarks and antiquarks in the target and (ii) production of quark-antiquark pairs followed by interactions with the target. We first calculate structure functions of the free nucleon and develop a model for the quark spectral functions. In this model mechanism (ii) is responsible for the sea quark content of the nucleon while mechanism (i) governs the valence part of the nucleon structure functions. We find that the coherent interaction of $\bar{q}q$ pairs with nucleons in the nucleus leads to shadowing at small x and discuss this effect in detail. In the large x region DIS takes place mainly on a single nucleon. There we focus on the derivation of the convolution model. We point out that the off-shell properties of the bound nucleon structure function give rise to sizable nuclear effects.

PACS number(s): 13.60.Hb, 24.10.−i, 24.85.+p, 25.30.−c

I. INTRODUCTION

Deep-inelastic lepton scattering (DIS) on nuclei is a powerful tool to investigate the quark-gluon structure of nucleons in a nuclear environment. The cross section of this process is studied as a function of the Bjorken variable $x = Q^2/2M\nu$ and the squared four-momentum transfer $Q^2 = -q^2$, where M is the nucleon mass and ν is the photon energy in the laboratory frame. Accurate experimental data [1–7] are now available for a number of nuclear targets over a wide kinematical range, $5 \times 10^{-5} < x < 0.8$ and $0.03\,\mathrm{GeV}^2 < Q^2 < 200\,\mathrm{GeV}^2$. The data show nontrivial nuclear effects over the whole range of Bjorken x. At $x < 0.1$ one observes shadowing, i.e., a systematic reduction of the nuclear structure function F_2^A with respect to A times the free nucleon structure function F_2^N. A small enhancement of the ratio $R = F_2^A/AF_2^N$ is seen at $x \approx 0.2$ and a pronounced dip occurs in that ratio at $x \sim 0.5$. Finally, for $x > 0.7$ a large enhancement of R is observed.

Numerous models have been proposed to explain these effects (for recent reviews, see, e.g., Refs. [8–10]). So far, most theoretical models for nuclear DIS give separate descriptions of the regions of small $x < 0.1$ and large $x > 0.2$. The physical reason for such a division becomes apparent in the space-time analysis of the DIS process. In the laboratory frame the interaction of the virtual photon with the target can proceed in two possible ways (see Fig. 1):

(i) the photon is absorbed by a quark or antiquark in the target which picks up the large energy and momentum transfer;

(ii) the photon converts into a quark-antiquark pair which subsequently interacts with the target.

An analysis of the contributions (i) and (ii) reveals that the second mechanism dominates at small $x \ll 0.1$ (see, e.g., the discussion in [11–14]). For $x > 0.1$ both processes (i) and (ii) contribute. In order to understand
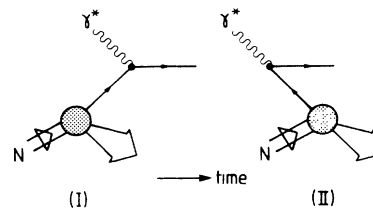
FIG. 1. Two basic mechanisms of deep-inelastic scattering.

the implications of this for nuclear targets let us consider characteristic space-time scales. Mechanism (i) has a characteristic scale which is determined by the size of the nucleon and does not depend on x. For mechanism (ii) the propagation length λ of the $q\bar{q}$ (or hadronic) fluctuations of the photon in the laboratory frame is $\lambda \sim (Mx)^{-1}$. For $x < 0.1$ this propagation length becomes larger than the average nucleon-nucleon distance in nuclei. As a consequence deep-inelastic scattering from nuclear targets at small x involves the coherent interaction of the pair with several nucleons in the nucleus. This leads to nuclear shadowing. Models of the shadowing effect in the laboratory frame [11–13,15–19] usually include mechanism (ii) only.

At large $x > 0.2$ effects resulting from coherent multiple scattering in the nucleus are not important since the space-time scales of both mechanisms (i) and (ii) are of the order of the nucleon size. In this region of x the virtual photon interacts incoherently with bound nucleons. Model descriptions of nuclear structure functions in the large $x > 0.2$ region [21–31] (for a review see [8,32]) usually start out from the impulse approximation in which both mechanisms (i) and (ii) are taken into account by using a phenomenological nucleon structure function. Results of such calculations show that nuclear binding and Fermi motion are responsible for the observed "old" EMC effect at large x.

The purpose of the present paper is to develop an approach to DIS which is based on a unified description of processes (i) and (ii). In Sec. II we develop a relativistically covariant formalism which incorporates the standard parton model but also permits us to include nonperturbative features which turn out to be important at small x. Our starting point is a general representation of structure functions in terms of dispersion integrals over quark spectral densities (Sec. II B). In Sec. III we develop a model for the quark spectral densities which separately reproduces the valence and sea quark parts of the free-nucleon structure functions. In Sec. IV we discuss nuclear structure functions. We find that shadowing at small x has a scaling contribution from mechanism (ii) (independent of Q^2) which turns out to be insufficient, however, to reproduce the empirical A dependence. At this point our results differ from those of Ref. [16]. We conclude that the propagation of strongly correlated $q\bar{q}$ pairs through the nucleus, partly in the form of vector

mesons, is important to reproduce the observed shadowing effect (Sec. IV A). For $x > 0.2$, where nuclear binding and Fermi motion are relevant, we discuss the limitations of the standard convolution model (Sec. IV B). We point out that there is no reason to ignore, as is usually done, the dependence of the structure functions on the invariant mass of the nucleon, p^2.

II. FRAMEWORK

According to the optical theorem, inclusive inelastic scattering of an electron/muon on a nucleon or nucleus can be described in terms of the forward scattering of a virtual photon. The amplitude for forward Compton scattering is

$$T_{\mu\nu}(P,q) = -i \int d^4\xi \, e^{iq\cdot\xi} \langle P|T(j_\mu(\xi)j_\nu(0))|P\rangle, \quad (1)$$

where q and P are the photon and target momenta, respectively. The electromagnetic current is denoted by j_μ. In what follows we shall discuss the scattering from an unpolarized target and assume that the average is taken over target polarization in Eq. (1). In this case there are only two independent terms in the Compton amplitude,

$$T_{\mu\nu}(P,q) = T_1(x,Q^2)\left(\frac{q_\mu q_\nu}{q^2} - g_{\mu\nu}\right) + \frac{T_2(x,Q^2)}{P\cdot q}L_\mu L_\nu, \quad (2)$$

where $Q^2 = -q^2$, $L_\mu = P_\mu - q_\mu P\cdot q/q^2$, and $x = Q^2/2P\cdot q$ is the Bjorken scaling variable [we use the normalization $\langle p|p'\rangle = (2\pi)^3 \, 2p_0\delta^{(3)}(\mathbf{p} - \mathbf{p}')$ both for fermions and bosons, so that the amplitudes T_1 and T_2 are dimensionless]. The structure functions F_1 and F_2 are given by the imaginary parts of the scalar amplitudes in (2):

$$F_{1,2}(x,Q^2) = -\frac{1}{2\pi}\,\mathrm{Im}\,T_{1,2}(x,Q^2). \quad (3)$$

It is commonly assumed that in the region of high momentum transfer, $Q^2 \gg M^2$, the main contribution to the Compton amplitude comes from the diagram, Fig. 2, in which the virtual photon couples to the quark current. Let us examine this contribution in detail. To leading order in Q^2 and in the axial gauge the Compton amplitude reads

$$T_{\mu\nu}(P,q) = -i \int \frac{d^4k}{(2\pi)^4} \sum_a e_a^2 \, \mathrm{Tr}\left[\Delta_a(k,P)\left(\gamma_\mu\frac{1}{\not{k}+\not{q}+i\epsilon}\gamma_\nu + \gamma_\nu\frac{1}{\not{k}-\not{q}+i\epsilon}\gamma_\mu\right)\right], \quad (4)$$

where the sum is taken over flavor and color degrees of freedom of the interacting quark which carries electric charge e_a. For simplicity we have dropped the quark mass in Eq. (4). Here $\Delta_a(k,P)$ is the Fourier transform of the correlator of the quark fields in the target,

$$\Delta_a(k,P) = -i \int d^4\xi \, e^{ik\cdot\xi} \langle P|T(\psi_a(\xi)\bar{\psi}_a(0))|P\rangle. \quad (5)$$
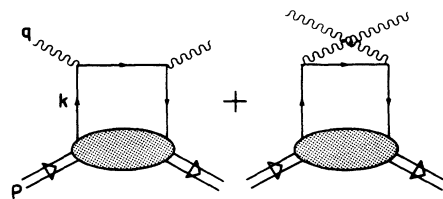

FIG. 2. Compton amplitude to the leading order in Q^2.

The structure functions can easily be found from Eq. (4) by applying appropriate projection operators. Neglecting terms of order $1/Q^2$ we find for the structure function F_2,

$$F_2(x) = x \sum_a e_a^2 \left[q_a(x) + \bar{q}_a(x) \right], \qquad (6)$$

where

$$q_a(x) = f_a(x), \qquad (7a)$$
$$\bar{q}_a(x) = -f_a(-x), \qquad (7b)$$

and

$$f_a(x) = -i \int \frac{d^4k}{(2\pi)^4} \frac{\text{Tr}(\not{q}\Delta_a(k,P))}{2P\cdot q} \delta\left(x - \frac{k\cdot q}{P\cdot q}\right). \qquad (8)$$

The two terms in Eq. (6) correspond to the direct and crossed terms of the Compton amplitude. It follows from Eq. (4) that the structure function F_1 is not independent; it is given by the Callan-Gross relation $F_2(x) = 2x\,F_1(x)$.

A. Parton model

Equation (8) gives a Lorentz-covariant representation of the quark distribution function which can be used in any reference frame. Here we first demonstrate that Eqs. (6) and (8) recover the familiar result of the parton model. Let us choose a reference frame in which the target moves with a large momentum $|\mathbf{P}| \to \infty$. In this frame the function $q_a(x)$ can be identified with the momentum distribution of quarks with flavor a in the target, and $\bar{q}_a(x)$ is the corresponding antiquark distribution. In order to see this we introduce a coordinate system such that the momentum transfer is $q = (0, \mathbf{0}_\perp, Q)$ (with $Q = \sqrt{Q^2}$). The hadron moves with momentum $P_3 = -Q/2x$ in the direction opposite the three-momentum transfer $\mathbf{q}$. Then Eq. (8) becomes

$$f(x) = -i \int \frac{d^3k}{(2\pi)^3} \delta\left(x - \frac{k_3}{P_3}\right) \int \frac{dk_0}{2\pi} \frac{\text{Tr}(\gamma_3 \Delta(k,P))}{2P_3}, \qquad (9)$$

where we have suppressed quark flavor and color indices for simplicity. It can be shown that $\gamma_3/P_3 = \gamma_0/P_0$ in Eq. (9), up to terms of order $M^2 x^2/Q^2$. We perform the k_0 integration by closing the integration contour in the upper half plane and obtain

$$-i \int \frac{dk_0}{2\pi} \frac{\text{Tr}(\gamma_0 \Delta(k,P))}{2P_0} = \int d^3r\, d^3r'\, e^{-i\mathbf{k}\cdot(\mathbf{r}-\mathbf{r}')} \times \langle \psi^\dagger(0,\mathbf{r}')\psi(0,\mathbf{r})\rangle. \qquad (10)$$

Here we have used translational invariance and introduced an additional space integration. The brackets in Eq. (10) denote $\langle \cdots \rangle = \langle P|\cdots|P\rangle/\langle P|P\rangle$. The right-hand side of Eq. (10) is, in fact, the momentum space density of quarks in the target. In order to clarify this connection further we expand the quark fields in terms of plane-wave spinors,

$$\psi(0,\mathbf{r}) = \sum_\sigma \int \frac{d^3k}{(2\pi)^3} \frac{1}{\sqrt{2|\mathbf{k}|}} \times \left[a(k,\sigma) u(k,\sigma) e^{i\mathbf{k}\cdot\mathbf{r}} + b^\dagger(k,\sigma) v(k,\sigma) e^{-i\mathbf{k}\cdot\mathbf{r}} \right], \qquad (11)$$

where $u(k,\sigma)$ is the Dirac spinor of a quark with momentum k and polarization σ, and $v(k,\sigma)$ is the corresponding antiquark spinor. The operators $a(k,\sigma)$ and $b(k,\sigma)$ acting on any physical state probe the momentum distribution of quarks and antiquarks in that state:

$$N(k) = \sum_\sigma \langle a^\dagger(k,\sigma) a(k,\sigma)\rangle, \qquad (12a)$$

$$\bar{N}(k) = \sum_\sigma \langle b^\dagger(k,\sigma) b(k,\sigma)\rangle. \qquad (12b)$$

Using the commutation relations between a, $a^\dagger$ and b, $b^\dagger$ and the orthogonality properties of spinors $u(k,\sigma)$ and $v(k,\sigma)$, we find from Eqs. (9) and (10)

$$f(x) = q(x) - \bar{q}(-x), \qquad (13)$$

where $q(x)$ and $\bar{q}(x)$ are the quark and antiquark distributions as functions of the target-momentum fraction,

$$q(x) = \int \frac{d^3k}{(2\pi)^3} \delta\left(x - \frac{k_3}{P_3}\right) N(\mathbf{k}), \qquad (14a)$$

$$\bar{q}(x) = \int \frac{d^3k}{(2\pi)^3} \delta\left(x - \frac{k_3}{P_3}\right) \bar{N}(\mathbf{k}). \qquad (14b)$$

The functions (14) have the usual simple interpretation: they represent the probability distributions of quarks $[q(x)]$ or antiquarks $[\bar{q}(x)]$ which carry a fraction x of the target longitudinal momentum. It is known from the parton-model analysis [33] that the probability of finding a parton moving backward $(x < 0)$ vanishes as $|\mathbf{P}| \to \infty$. Also, momentum conservation does not permit partons with $x > 1$. Therefore the functions $q(x)$ and $\bar{q}(x)$ vanish outside the physical interval $0 \le x \le 1$.

B. Structure functions as dispersion integrals

Our primary task is to study deep-inelastic scattering off nuclei. In this case the simplicity of the parton model is lost, because no reliable approach exists to deal with nuclear systems in the infinite-momentum frame. For this purpose the preferable frame of reference is the laboratory system. In the present paper we describe the distribution function $f(x)$ using the analytical properties of the quark correlator (5). This method preserves relativistic covariance and can therefore be used in any frame.

Following Refs. [34,35] we assume that the quark correlator Δ is an analytic function of the variables $s = (P - k)^2$, $u = (P + k)^2$, and k^2. For real s and u the quark correlator has a right-hand cut in the variable s, a left-hand cut in the variable u, and singularities

for $k^2 > 0$. In order to make use of these analytical properties of Δ in the loop integral (8), it is convenient to parametrize the loop momentum k in terms of the external momenta P and q (introducing the Sudakov variables):

$$k = \alpha P + \beta q' + k_\perp, \qquad (15)$$

where $q' = xP + q$, and $k_\perp$ is a two-dimensional vector (with $k_\perp^2 < 0$) perpendicular to both P and q.

The integration with respect to β can be done using the analytic properties, just mentioned, of the quark correlator. As a result one finds that the distribution function $f(x)$ vanishes outside the physical interval $|x| \leq 1$ as it should. For $0 \leq x \leq 1$ the distribution function $f(x)$ [or $q(x)$] is given by a dispersion integral in the variable s along the right-hand cut. For $-1 \leq x \leq 0$ the u-channel cut is relevant. In order to represent the structure functions in this way we introduce functions $\rho_{R,L}$ for the imaginary parts taken along the right-hand cut (R) and left-hand cut (L) as follows:

$$\rho_R(s, k^2, \alpha) = \frac{\mathrm{Im}_R \, \mathrm{Tr}(\slashed{q}\Delta(k, P))}{2\pi \, P \cdot q}, \qquad (16a)$$

$$\rho_L(u, k^2, \alpha) = \frac{\mathrm{Im}_L \, \mathrm{Tr}(\slashed{q}\Delta(k, P))}{2\pi \, P \cdot q}. \qquad (16b)$$

In terms of these functions the quark distribution $q(x)$ and the antiquark distribution $\bar{q}(x)$ are

$$q(x) = \frac{1}{1-x} \int \frac{ds \, d^2 k_\perp}{2(2\pi)^3} \, \rho_R(s, k^2, x), \qquad (17a)$$

$$\bar{q}(x) = \frac{-1}{1-x} \int \frac{du \, d^2 k_\perp}{2(2\pi)^3} \, \rho_L(u, k^2, -x), \qquad (17b)$$

where we have suppressed the flavor indices again. The squared quark four-momentum k^2 is

$$k^2 = x \left(\frac{s}{x-1} + M^2 \right) + \frac{k_\perp^2}{1-x} \qquad (18)$$

in Eq. (17a), and an analogous expression holds with s replaced by u for the antiquark distribution $\bar{q}(x)$ in Eq. (17b).

The spectral densities (16) can be written in terms of spectral sums over a complete set of intermediate states inserted between the two quark field operators in Eq. (5). In order to write the spectral representation in a more explicit form we introduce matrix elements of the quark field operator taken between the nucleon and some intermediate state, $\psi_n(\mathbf{K}) = \langle \mathbf{K}, n | \psi(0) | P \rangle$ and $\bar{\psi}_m(\mathbf{K}) = \langle P | \psi(0) | m, \mathbf{K} \rangle$. Intermediate states are labeled by their total momentum $\mathbf{K}$ and other quantum numbers denoted by n or m. In terms of the amplitudes ψ_n and $\bar{\psi}_m$ the spectral densities (16) can then be expressed as follows:

$$\rho_R(s, k^2, \alpha) = \frac{1}{2P \cdot q} \sum_n \bar{\psi}_n(\mathbf{P}-\mathbf{k}) \slashed{q} \psi_n(\mathbf{P}-\mathbf{k})$$

$$\times \delta(s - M_n^2), \qquad (19)$$

$$-\rho_L(u, k^2, -\alpha) = \frac{1}{2P \cdot q} \sum_m \bar{\psi}_m(\mathbf{P}-\mathbf{k}) \slashed{q} \psi_m(\mathbf{P}-\mathbf{k})$$

$$\times \delta(u - M_m^2). \qquad (20)$$

Here M_n^2 and M_m^2 are the invariant masses of the intermediate states. Note that Eqs. (19) and (20) correspond to two different time orderings of the quark operators in (5).

The basic assumption is now that the spectral densities vanish at large k^2 so that integrals in Eqs. (17) are convergent and dominated by the region of $k^2 \sim \bar{m}^2$, where $\bar{m}$ is a characteristic hadronic mass scale. It follows from Eq. (18) that the behavior of the quark distributions at $x \to 1$ is given by the asymptotics of the spectral densities at $k^2 \to -\infty$. At small x the k^2 is finite even for large $s \sim \bar{m}^2/x$. Therefore for small x the integral in Eqs. (17) is sensitive to the high-energy parts of the spectral densities. In the region of intermediate or large $x > 0.2$ the region of finite $s \sim \bar{m}^2$ is of major importance.

The spectral representation [(19) and (20)] offers a convenient way to separate contributions from mechanisms (i) and (ii). To see this, consider the amplitude ψ_n in the laboratory frame, with target momentum $P = (M, \mathbf{0})$. The quark field operator acting on the target state can either annihilate a quark in the target or create an antiquark. In the former case the amplitude $\psi_n \propto \langle -\mathbf{k}, n | a(k) | P \rangle$ describes the absorption of a virtual photon by quarks with momentum $\mathbf{k}$. This contribution corresponds to the mechanism (i). The contribution from the antiquark part of the ψ operator, $\psi_n \propto \langle -\mathbf{k}, n | b^\dagger(-k) | P \rangle$, corresponds to the mechanism (ii). This part of the amplitude ψ_n describes the "external" antiquarks from $q\bar{q}$ fluctuations of the virtual photon and their interaction with the target. The amplitude $\bar{\psi}_m$ also has two parts: one associated with contributions from antiquarks bound to the target $[\bar{\psi}_m^\dagger \propto \langle -\mathbf{k}, m | b(k) | P \rangle]$, and the other one from "external" quarks coming from the photon wave function, $[\bar{\psi}_m^\dagger \propto \langle -\mathbf{k}, m | a^\dagger(-k) | P \rangle]$.

III. QUARK SPECTRAL DENSITIES AND NUCLEON STRUCTURE FUNCTIONS

In this section we construct nucleon structure functions using a model for the quark spectral densities ρ_L and ρ_R. We further elaborate the concept, appropriate in the laboratory frame, that the full quark spectral function can be divided into two parts corresponding to mechanisms (i) and (ii), as illustrated in Fig. 1.

The part of the spectral density that describes mechanism (i) is proportional to the probability to find a quark with four-momentum k in the nucleon. The characteristic momenta of quarks bound in the nucleon are of the order of the nucleon mass, $k \sim M$. Therefore the main contributions to the spectral densities from mechanism (i) come from the region $|k^2| \sim M^2$ and $s \sim M^2$. This kinematical region determines the behavior of structure functions at $x > 0.2$.

On the other hand, contributions to the quark spec-

tral densities from mechanism (ii) rise with s (or u). In fact, the matrix element $\langle \mathbf{k}, n|b^\dagger(k)|P\rangle$ describes scattering of an antiquark with momentum $\mathbf{k}$ from the nucleon, with transition of the system to the final state $|n, \mathbf{k}\rangle$. The possible antiquark momenta $\mathbf{k}$ are determined by the wave function of the photon and can be as large as the photon momentum $\mathbf{q}$. Therefore, the invariant mass of the antiquark-nucleon system is large, $s \gg M^2$. Due to unitarity, the sum over all states n in Eq. (19) will be proportional to the antiquark-nucleon forward elastic scattering amplitude. It is known from Regge theory that imaginary parts of amplitudes rise with energy as s^{α_P}, where α_P is the intercept of the Pomeron. Therefore contributions to the spectral density from mechanism (ii) grow with energy and dominate at large s. This mechanism determines the small x part of structure functions.

A. Model for quark spectral densities

With this discussion in mind we now develop the following simple model for the quark spectral densities. We introduce a parameter s_0 which separates the full spectrum into a low-energy $(s < s_0)$ part and a high-energy $(s > s_0)$ part. We assume furthermore that the low-energy part of the spectrum is dominated by mechanism (i), while the high-energy part is given by mechanism (ii) (for illustration see Fig. 3):

$$\rho(s, k^2) = \rho^{(i)}(s, k^2)\theta(s_0 - s) + \rho^{(ii)}(s, k^2)\theta(s - s_0).$$

$$(21)$$

For the low-energy part of the spectrum $(s < s_0)$ we make the following ansatz:

$$\rho_R^{(i)}(s, k^2) = \Phi(k^2)\delta(s - \bar{s}), \qquad (22)$$

together with $\rho_L = 0$ in this region, which implies that we neglect contributions to spectral densities coming from antiquarks in the nucleon. This choice can be motivated within a constituent quark picture of the nucleon. In this case $\sqrt{\bar{s}} \approx \frac{2}{3}M$ is an average mass of the residual two-quark intermediate state, and $\Phi(k^2)$ is the squared momentum space wave function of the constituent quark. Here we will not confine ourselves to some particular model, but rather choose the spectral density at small values of s in such a way that we reproduce the measured valence quark distribution. The contribution from Eq. (22) to the deep-inelastic structure function is
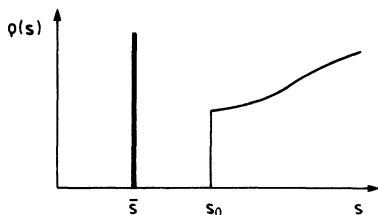
$$q^{(i)}(x) = \frac{1}{16\pi^2} \int_{-\infty}^{k_{\max}^2(\bar{s}, x)} dk^2 \, \Phi(k^2), \qquad (23)$$

where $k_{\max}^2(s, x)$ is the maximum value of the squared quark four-momentum for given values of s and x,

$$k_{\max}^2(s, x) = x\left(\frac{s}{x - 1} + M^2\right). \qquad (24)$$

In order to describe the region of large $s > s_0$ we introduce the quark-nucleon forward-scattering amplitude $T(k, P)$ as follows:

$$\Delta(k, P) = \frac{1}{\not{k} - m_q + i\epsilon} \, T(k, P) \, \frac{1}{\not{k} - m_q + i\epsilon}. \qquad (25)$$

The quantity relevant for the calculation of the quark spectral densities (16) is $\mathrm{Tr}(\gamma_\mu \Delta)$. In terms of the amplitude T this trace can be written as follows:

$$\mathrm{Tr}(\gamma_\mu \Delta(k, P)) = (k^2 - m_q^2)^{-2}$$
$$\times \left[4k_\mu \overline{T} + (m_q^2 - k^2)\,\mathrm{Tr}(\gamma_\mu T)\right], \quad (26)$$

where $\overline{T} = \frac{1}{2}\mathrm{Tr}[(\not{k} + m_q)T(k, P)]$ is the amplitude averaged over the quark spin. When examining the Dirac structure of T, we find that only a scalar term and a term proportional to the γ matrix contribute to (26). One can neglect the scalar term because its contribution to the amplitude $\overline{T}$ is proportional to the quark mass m_q. The leading contribution to the amplitude $\overline{T}$, the one which rises with s, comes from the term proportional to $\gamma \cdot P$. Based on these arguments we write the amplitude T as

$$T(k, P) = C(s, u, k^2)\not{P}, \qquad (27)$$

where C is a Lorentz-invariant function of s, u, and k^2, which is related to the spin-averaged amplitude $\overline{T}$ as follows:

$$\overline{T}(s, u, k^2) = \frac{1}{2}(u - s)C(s, u, k^2). \qquad (28)$$

We emphasize here that the amplitude $\overline{T}(s, u, k^2)$ describes both the qN- and the $\bar{q}N$-scattering channels. In the s channel $\overline{T}(s, u, k^2)$ coincides with the antiquark-nucleon scattering amplitude $T_{\bar{q}N}(s, k^2)$, while in the u channel $\overline{T}(s, u, k^2)$ gives the quark-nucleon amplitude $T_{qN}(u, k^2)$.

We are now prepared to calculate the contribution from mechanism (ii) to the quark spectral densities (16) and to the quark and antiquark distributions (17). Using Eqs. (26), (27), and (28) we obtain[1]

FIG. 3. A schematic picture of the quark spectral function.

---

[1] As compared to the spinless case discussed in [16], the spin 1/2 distributions have a generic factor of 2 which reflects the number of spin degrees of freedom, and the term in brackets under the integral replaced the factor x.

$$q^{(ii)}(x) = \frac{1}{(2\pi)^3} \int_{s_0}^{\infty} ds \int_{-\infty}^{k^2_{max}(s,x)} dk^2 \frac{Im T_{\bar{q}N}(s,k^2)}{(k^2 - m_q^2)^2} \left(-x + \frac{m_q^2 - k^2}{s - M^2 - k^2} \right),$$ (29a)

$$\bar{q}^{(ii)}(x) = \frac{1}{(2\pi)^3} \int_{s_0}^{\infty} du \int_{-\infty}^{k^2_{max}(u,x)} dk^2 \frac{Im T_{qN}(u,k^2)}{(k^2 - m_q^2)^2} \left(-x + \frac{m_q^2 - k^2}{u - M^2 - k^2} \right),$$ (29b)

where we have introduced an integration over the squared quark four-momentum k^2 instead of integration over transverse momentum $k_\perp$.

In what follows we shall consider the structure function F_2 of an isoscalar nucleon, $F_2^N = \frac{1}{2}(F_2^p + F_2^n)$. Isospin symmetry implies that F_2^N is proportional to the flavor singlet combination of quark and antiquark distributions,

$$F_2^N(x) = \frac{5}{18}x \sum_a [q_a(x) + \bar{q}_a(x)].$$ (30)

(Here we have assumed that the difference between strange and charmed sea is negligibly small.) In our model the quark and antiquark distributions are given by

$$\sum_a [q_a(x) + \bar{q}_a(x)]$$
$$= q^{(i)}(x) + N_f N_c \left[q^{(ii)}(x) + \bar{q}^{(ii)}(x) \right],$$ (31)

where $q^{(i)}$ is given by Eq. (23) and represents the sum of quark distributions of different flavors due to the mechanism (i). The quantities $q^{(ii)}$ and $\bar{q}^{(ii)}$ are the quark and antiquark distributions related to mechanism (ii), averaged over flavor and color. They are given by Eqs. (29), where T_{qN} and $T_{\bar{q}N}$ are quark-nucleon amplitudes averaged over quark spin, flavor, and color. We have $N_f = 4$ and $N_c = 3$.

The valence quark distribution is measured in neutrino scattering in terms of the structure function $F_3(x)$. In our model it is given by

$$F_3^N(x) = q^{(i)}(x) + N_f N_c \left[q^{(ii)}(x) - \bar{q}^{(ii)}(x) \right].$$ (32)

This structure function is normalized to the number of valence quarks in the nucleon.

B. Quark-nucleon amplitude

In order to specify $q^{(ii)}$ and $\bar{q}^{(ii)}$ we note that the amplitudes T_{qN} and $T_{\bar{q}N}$ can be connected to observable proton-proton and antiproton-proton forward-scattering amplitudes. We recall the well-known phenomenological fact that total hadronic cross sections at high energies are proportional to the number of constituent quarks in hadrons [33]. Hence the forward proton-proton amplitude can be written in terms of the quark-proton amplitude in the laboratory frame as

$$\frac{T_{pp}(S)}{S} = 3 \left\langle \frac{T_{qp}(yS, k^2)}{yS} \right\rangle.$$ (33)

Here S is the squared proton-proton center-of-mass energy, k is the four-momentum of a constituent quark in the target, and y is the fraction of the target light-cone momentum carried by the constituent quark. A similar equation relates the antiquark-proton amplitude $T_{\bar{q}p}$ to the antiproton-proton forward-scattering amplitude $T_{\bar{p}p}$. In the laboratory frame $y = (k_0 + k_3)/M$, $k_0 = M - \sqrt{m_R^2 + \mathbf{k}^2}$, where m_R is the mass of the spectator system. The averaging in Eq. (33) is performed over the spectral function of the constituent quarks in the proton target. In order to estimate typical values of y and k^2 we assume $m_R \approx \frac{2}{3}M$. This gives average values $\bar{y} \approx 0.3$ and $\overline{k^2} = \langle k_0^2 - \mathbf{k}^2 \rangle \approx -0.1$ GeV^2.

The constituent quark-nucleon scattering amplitudes in (33) might, in principle, be different from the quark-nucleon amplitudes entering in Eqs. (29). However, at small values of x, the quark-nucleon center-of-mass energy s in Eq. (29) will be of the order of $s \sim 1$ GeV$^2/x$. As a consequence the typical formation time of a constituent quark will be $\tau_F \sim |k_0|/m_q^2 \sim s/2m_q^2 M \sim 1/Mx$. This is comparable to the propagation length $\lambda \sim 1/Mx$ of the $q\bar{q}$ pair in the photon wave function. We can therefore assume that at small x the quark-nucleon amplitudes which enter in the quark distribution functions can be approximated by the constituent quark-nucleon amplitudes determined by hadron-nucleon scattering.

Through Eq. (33) the s dependence of the quark-nucleon and antiquark-nucleon amplitudes T_{qN} and $T_{\bar{q}N}$ is fixed. Above the resonance region the pp and $\bar{p}p$ amplitudes are well reproduced by Pomeron exchange with an intercept $\alpha_P = 1 + \epsilon$, and by exchange of two Regge trajectories corresponding to the ω and the f mesons with intercepts $\alpha_\omega = \alpha_f = \alpha_R \approx 1/2$. The forward-scattering amplitudes can then be written as [36]

$$T_{pp}(S) = R_P S^{\alpha_P} \left(i + \tan \frac{\pi\epsilon}{2} \right)$$
$$+ S^{\alpha_R} \left(iR_\Delta - \frac{R_\Sigma + R_\Delta \cos \pi\alpha_R}{\sin \pi\alpha_R} \right),$$ (34a)

$$T_{\bar{p}p}(S) = R_P S^{\alpha_P} \left(i + \tan \frac{\pi\epsilon}{2} \right)$$
$$+ S^{\alpha_R} \left(iR_\Sigma - \frac{R_\Delta + R_\Sigma \cos \pi\alpha_R}{\sin \pi\alpha_R} \right),$$ (34b)

where R_P is the residue of the Pomeron, while R_Σ and R_Δ stand for the sum and the difference of residues of the f and ω trajectories. In the following we shall use the best fit parameters of Ref. [37]:

$$\epsilon = 0.0808, \quad R_P = 21.70\,\text{mb/GeV}^{2\epsilon},$$
$$\alpha_R = 0.5475, \quad R_\Delta = 56.08\,\text{mb GeV}^{(1-\alpha_R)},$$
$$R_\Sigma = 98.39\,\text{mb GeV}^{(1-\alpha_R)}.$$

The amplitudes T_{qN} and $T_{\bar{q}N}$ should depend not only on s, but also on the squared quark four-momentum k^2. We assume that the k^2 behavior of the Pomeron and Reggeon parts of the amplitudes is given as

$$T_{qN}(s, k^2) = g_P(k^2)T_{qN}^P(s, 0) + g_R(k^2)T_{qN}^R(s, 0), \quad (35)$$

with functions $g_{P,R}(k^2)$ for which we chose the following ansatz:

$$g_{P,R}(k^2) = (1 - k^2/\Lambda_{P,R}^2)^{-n_{P,R}}, \quad (36)$$

with momentum-space cutoffs Λ_P, Λ_R and exponents n_P and n_R.

C. Nucleon structure functions at large Q^2

In this section we determine $g_P(k^2)$ and $g_R(k^2)$ and other remaining parameters such that we reproduce the measured structure functions in the scaling region. This involves the antiquark distributions $\bar{q}(x)$ [Eq. (29) in our model] together with the structure functions $F_2^N(x)$ and $F_3^N(x)$ [Eqs. (30) and (32)].

The valence quark distribution is mainly given in terms of the momentum distribution $\Phi(k^2)$ in Eq. (22), which still needs to be specified. We use the ansatz

$$\Phi(k^2) = \Phi(0) \, (1 - k^2/\Lambda_V^2)^{-n_V}, \quad (37)$$

with a suitable cutoff parameter Λ_V and a characteristic exponent n_V. The normalization constant $\Phi(0)$ is determined through the number of valence quarks in the target.

From Eqs. (17) and (18) it follows that the asymptotic behavior of the quark spectral functions at $k^2 \to -\infty$ determines the structure functions at $x \to 1$. Indeed, our model gives

$$q^{(i)}(x \to 1) \propto (1 - x)^{n_V - 1}, \quad (38a)$$

$$q^{(ii)}(x \to 1) \propto (1 - x)^{n_{P,R} + 1}. \quad (38b)$$

The quark counting rule [33,38,39] for the valence distribution requires $q^{(i)}(x \to 1) \propto (1 - x)^3$, which fixes $n_V = 4$. Furthermore, the sea quark distribution should approach zero at $x \to 1$ with a high power in $(1 - x)$. We find that the Pomeron and Reggeon exponents $n_P = n_R = 4$, which correspond to a $(1 - x)^5$ behavior at large x, give a good fit to $\bar{q}(x)$.

The Regge parameters of the quark-nucleon and antiquark-nucleon amplitude in Eqs. (29) are already fixed at an averaged squared momentum $|k^2| \sim 0.1 \, \text{GeV}^2$ by employing Eq. (33). Note that the overall magnitudes of the type (ii) quark and antiquark distributions (29) are set by the qN and $\bar{q}N$ cross sections. Using Eq. (33) we find $\sigma_{\bar{q}N} \approx \sigma_{qN} \approx \frac{1}{3}\sigma_{pp} \approx 13 \, \text{mb}$ at high energy. The remaining scales enter through the cutoffs in $g_{P,R}(k^2)$ and $\Phi(k^2)$, together with $\bar{s}$ and s_0, which separates high and low energy parts of the quark spectral density (21,22). These parameters are determined by fits to the nucleon structure functions at large Q^2. In our analysis we use recent NMC data [40] for $F_2(x)$
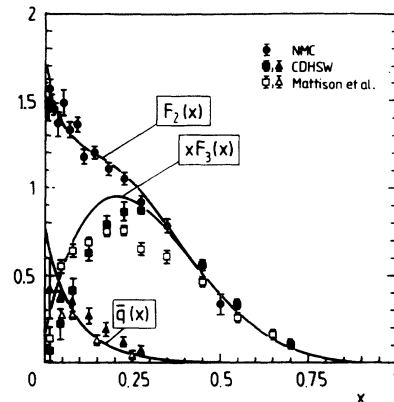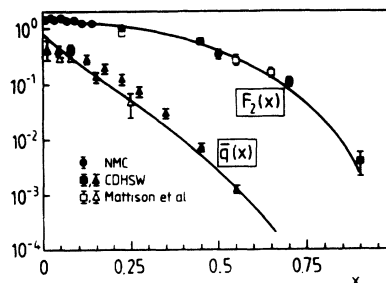

FIG. 4. The nucleon structure functions $F_2^N(x)$, $F_3^N(x)$, and the antiquark distribution $\bar{q}(x)$. Experimental data for the $F_2^N(x)$ (circles) are from Ref. [40], for $F_3^N(x)$ (squares) and $\bar{q}(x)$ (triangles) from Refs. [41,42].
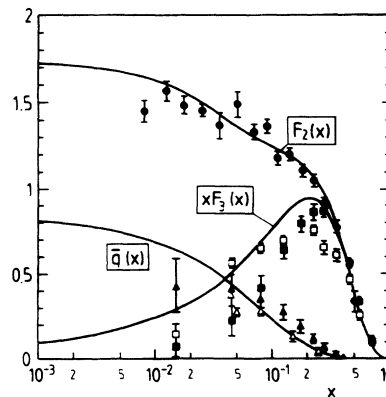
and neutrino data [41,42] for $F_2^N(x)$, $xF_3^N(x)$, and $\bar{q}(x)$ at average momentum transfer $Q^2 \approx 5 - 10 \, \text{GeV}^2$. Our result shown in Fig. 4 uses

$$\begin{aligned} \Lambda_V^2 &= 1.2 \, \text{GeV}^2, \\ \Lambda_P^2 &= 2.5 \, \text{GeV}^2, \\ \Lambda_R^2 &= 4.0 \, \text{GeV}^2, \end{aligned} \quad (39)$$

together with

(a)

(b)

FIG. 5. The nucleon structure functions $F_2^N(x)$, $F_3^N(x)$, and $\bar{q}(x)$ at large (a) and small (b) values of the Bjorken variable x.

$$s_0 = 2\bar{s} = 4\,\text{GeV}^2. \tag{40}$$

The global view in Fig. 4 is supplemented by more detailed comparisons with data at large x [Fig. 5(a)] and at small x [Fig. 5(b)]. In particular, Fig. 5(a) demonstrates that the exponents $n_V = n_P = n_R = 4$ are properly chosen to reproduce tails of the distribution functions, while Fig. 5(b) focuses on the behavior at $x < 0.1$ where sea quarks begin to dominate F_2^N.

A remark concerning the value of $\bar{s}$ is in order. This parameter roughly corresponds to the average squared mass of the residual quark-gluon system, with one quark removed from the nucleon. The value of $\bar{s}$ depends on the scale at which we study the system. For example, in the bag model (or in a constituent quark model) $\sqrt{\bar{s}} \sim \frac{2}{3}M$, where M is the nucleon mass. This corresponds to the quark distributions at a low resolution scale $Q^2 < 1\,\text{GeV}^2$, which then has to be evolved to the momentum transfer Q^2 at which the experimental data are taken (e.g., [43]). In terms of the quark spectral densities [(19) and (20)] the Q^2-evolution effect modifies the spectrum of intermediate states by adding radiative corrections which generate gluons and $q\bar{q}$ pairs. This shifts the quark spectra to larger values of s. In our approach we fit to the measured structure functions at large Q^2 and effectively incorporate the Q^2-evolution effect in the parameter $\bar{s}$, averaged over the Q^2 range of the experimental data.

D. Structure function at small Q^2 and small x

So far, we have only discussed the scaling region, $Q^2 > 5\,\text{GeV}^2$. New phenomena enter at small Q^2 and small x. This is also where shadowing effects show up in the nuclear structure functions F_2^A, so that special attention is assigned to this region.

At small $Q^2 < 1\,\text{GeV}^2$ the scaling behavior is violated. Furthermore, conservation of the electromagnetic current requires that F_2 must vanish as Q^2 goes to zero. We therefore need a model which provides a smooth transition from the scaling to nonscaling regions. Here we discuss a model based on the generalized vector-meson dominance (GVMD) ideas [11]. In the GVMD approach the structure function F_2 at small $x < 0.1$ is expressed in terms of a dimensionless spectral function $\Pi(\mu^2)$ of hadronic states which couple to the photon:

$$F_2^N(x, Q^2) = \frac{Q^2}{\pi} \int_0^\infty d\mu^2 \, \frac{\mu^2 \Pi(\mu^2)}{(\mu^2 + Q^2)^2} \, \sigma_N(\mu^2, S). \tag{41}$$

Here $\sigma_N(\mu^2, S)$ is the cross section for scattering of a hadronic state with mass μ from the nucleon, and $S = M^2 + Q^2(1/x - 1)$ is the total squared center-of-mass

TABLE I. Vector-meson masses m_V [44], coupling constants g_V [45], and cross sections σ_{VN} [46].

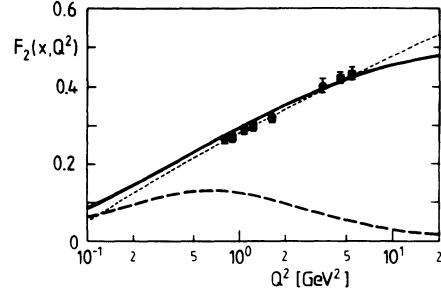| V	m_V (MeV)	$g_V^2/4\pi$	σ_{VN} (mb)
ρ	768.3	2.38	27
ω	782.0	18.4	27
ϕ	1019.4	13.8	12

FIG. 6. The Q^2 behavior of $F_2^N(x, Q^2)$ at small x. The data points are from Ref. [40] at $x = 0.008$ (circles) and $x = 0.0175$ (squares). The contribution from vector mesons (43) is shown by the dashed line. The solid curve is the full result using Eq. (44). The dotted line is the result for $F_2^N(x = 0.01, Q^2)$ using an empirical parametrization of the NMC data [40].

energy of the virtual photon-nucleon system. The distribution Π represents the spectrum of correlated quark-antiquark pairs and multimeson states with spin and parity $J^\pi = 1^-$. It separates into a low-mass part dominated by the vector mesons and a high-mass continuum part Π_c:

$$\Pi(\mu^2) = \sum_{V=\rho,\omega,\phi} \left(\frac{m_V^2}{g_V^2}\right) \delta(\mu^2 - m_V^2)$$
$$+ \Pi_c(\mu^2)\theta(\mu^2 - \mu_0^2), \tag{42}$$

where the continuum starts at $\mu_0 \gtrsim 1\,\text{GeV}$, just above the ϕ-meson mass. For the vector-meson masses m_V, their coupling constants g_V and cross sections σ_{VN} we use standard values summarized in Table I.

The vector-meson part is then

$$F_2^{N,\text{VM}} = \frac{Q^2}{\pi} \sum_{V=\rho,\omega,\phi} \left(\frac{m_V^2}{g_V}\right)^2 \left(\frac{1}{m_V^2 + Q^2}\right)^2 \sigma_{VN}. \tag{43}$$

It dominates the structure function at small $Q^2 < 1\,\text{GeV}^2$. On the other hand, at large momentum transfer $Q^2 \gg m_V^2$ the vector-meson contribution (43) vanishes as $\sim m_V^2/Q^2$. In this region large masses $\mu^2 \sim Q^2$ in the Π_c part of the spectral function (42) take over. At large $Q^2 \gg \mu_0^2$ this piece leads to a structure function with proper scaling behavior.

With this consideration in mind, we make the following ansatz in order to interpolate between the regions of small and large Q^2 at $x < 0.1$:[2]

$$F_2^N(x, Q^2) = F_2^{N,\text{VM}}(x, Q^2) + \frac{Q^2}{Q^2 + Q_0^2} F_2^{N,\text{as}}(x). \tag{44}$$

For the asymptotic part $F_2^{N,\text{as}}(x)$ of the structure func-

---

[2]Equation (44) is similar to a structure function model discussed in [47].

tion we use our model as described in the previous section. The parameter Q_0^2 is expected to be of order $\mu_0^2 \sim 1$ GeV^2. Scaling occurs for $Q^2 \gg Q_0^2$.

In Fig. 6 we show the characteristic behavior of $F_2^N(x, Q^2)$ at a small value of the Bjorken variable ($x = 0.01$) as a function of Q^2. We find that $Q_0^2 = 2$ GeV^2 gives a good description of the data. One observes that vector mesons dominate at $Q^2 \ll 1$ GeV^2, whereas the scattering of uncorrelated $q\bar{q}$ pairs governs F_2^N for $Q^2 > 2$ GeV^2. At $Q^2 = 1$ GeV^2, roughly one third of F_2^N at $x = 0.01$ is due to vector mesons; at $Q^2 = 5$ GeV^2 they still contribute about 10%. This is in agreement with results obtained within the framework of the generalized vector-meson dominance model [11].

IV. NUCLEAR STRUCTURE FUNCTIONS

We now turn to our main theme, namely DIS on nuclear targets and the structure function $F_2^A(x, Q^2)$.

Let us first discuss the region of small x. We have pointed out that deep-inelastic scattering at small x (as seen from the target rest frame) proceeds dominantly via the mechanism (ii), and we now investigate nuclear effects based on this observation. As we already mentioned, for $x < 0.1$ the propagation length $\lambda \sim (Mx)^{-1}$ of $q\bar{q}$ fluctuations in the photon wave function exceeds the average distance $d \sim 1.8$ fm between bound nucleons in the nucleus. The propagating $q\bar{q}$ pair can then interact coherently with several nucleons. This multiple scattering effect becomes significant when λ is larger than the quark mean free path $l = (\rho\sigma_{qN})^{-1}$, where ρ is the average nuclear density. In terms of the x variable the last condition reads $x < \rho\sigma_{qN}/M$. The nuclear effects due to multiple scattering of the $q\bar{q}$ pair will saturate for $x < (MR_A)^{-1}$, i.e., when the propagation length λ exceeds the nuclear radius R_A. In this case the virtual photon converts into a $q\bar{q}$ pair already outside the nucleus. This pair interacts with nucleons at the nuclear surface which absorbs part of the incoming flux and thereby screens the inner nucleons. This is the *shadowing* effect which we study in detail in the next section.

On the other hand, coherent multiple scattering effects are not important at large x where $\lambda < d$ and the $q\bar{q}$ fluctuation has no time to scatter more than once. In this region the DIS process takes place mainly on a single nucleon in the nucleus. Effects due to nuclear binding and Fermi motion are now important. We discuss these in detail in Sec. IV B.

A. The small x region: Shadowing

As in our previous discussion of the free-nucleon structure function F_2^N, we use the following ansatz for the nuclear structure function:

$$F_2^A(x, Q^2) = F_2^{A,\text{VM}}(x, Q^2) + \frac{Q^2}{Q^2 + Q_0^2} F_2^{A,\text{as}}(x), \quad (45)$$

and discuss the asymptotic (scaling) and vector-meson

contributions to F_2^A separately.

Consider first the scaling part $F_2^{A,\text{as}}(x)$. It is formally obtained from $F_2^N(x)$ in our model through the replacement of the quark-nucleon and antiquark-nucleon amplitudes T_{qN} and $T_{\bar{q}N}$ in Eqs. (29) by corresponding nuclear amplitudes, T_{qA} and $T_{\bar{q}A}$. For the type (i) distributions in Eq. (31) we simply use $q_A^{(i)}(x) = Aq_N^{(i)}(x)$; the validity of this approximation will be discussed in the next section. We use Glauber multiple scattering theory [48] to express the nuclear amplitudes T_A in terms of the T_N:

$$T_A(s, t)$$
$$= -2is \int d^2\mathbf{b}\, e^{i\mathbf{q}'\cdot\mathbf{b}} \langle A| \exp\left(i\sum_j \chi(\mathbf{b} - \mathbf{b}_j)\right) - 1|A\rangle.$$
$$(46)$$

Here the averaging is performed over the nuclear wave function and the sum runs over all bound nucleons located at positions $\mathbf{r}_j = (\mathbf{b}_j, z_j)$ in the nuclear c.m. frame; $\mathbf{q}'$ is the momentum transfer, $t = -\mathbf{q}'^2$. The eikonal phase $\chi(\mathbf{b})$ is related to the nucleon amplitude T_N as follows:

$$T_N(s, t) = -2is \int d^2\mathbf{b}\, e^{i\mathbf{q}'\cdot\mathbf{b}} \{\exp[i\chi(\mathbf{b})] - 1\}. \quad (47)$$

The Glauber analysis of high-energy hadron scattering from nuclei indicates that the result for T_A is not sensitive to NN correlations and other details of the nuclear wave function [49]. We can therefore evaluate the nuclear matrix element in Eq. (46) in a simple approximation assuming that the squared nuclear wave function is given by the product of Gaussian one-particle densities:

$$|\Psi_A(\mathbf{r}_1, \ldots, \mathbf{r}_A)|^2 = \prod_{j=1}^{A} (\pi R^2)^{-3/2} \exp(-r_j^2/R^2). \quad (48)$$

The parameter $R^2 = \frac{2}{3}R_A^2$ is fixed by the nuclear-root mean-square radius $R_A = 1.12 A^{1/3}$ fm as determined by electron scattering data. Using this wave function one can easily calculate T_A in terms of T_N, with the result

$$T_A(s, k^2) = T_N(s, k^2) \sum_{j=1}^{A} \frac{1}{j}\binom{A}{j}\left[\frac{iT_N(s, k^2)}{2\pi s R^2}\right]^{j-1}. \quad (49)$$

The effective number n_{eff} of terms which contribute to the sum (49) can be estimated as the average number of rescatterings of a classical particle moving along the diameter of the nucleus: $n_{\text{eff}} = 2R/l$, where l is the quark mean free path, and $l \approx 3$ fm for a quark-nucleon cross section $\sigma_{qN} \approx 13$ mb. Therefore the triple scattering term $j = 3$ practically saturates the multiple scattering series for nuclei up to $A \sim 100$. In the actual calculations we keep four terms in Eq. (49).

The calculated ratios $F_2^{A,\text{as}}(x)/AF_2^{N,\text{as}}(x)$ are shown as dashed curves in Fig. 7 for several nuclei. Comparing these results with the recent NMC data [2], we find that roughly only half of the measured shadowing effect can be explained in this way. In other words, mechanism (ii) alone, with quark- and antiquark-nucleon interactions

constrained by high energy pp and $p\bar{p}$ data, cannot account for all of the observed nuclear shadowing.

We find this not surprising, for the following reason. The experimental data at small x are taken at relatively small values of Q^2, while the dashed curve in Fig. 7 corresponds to large $Q^2 > 5$ GeV^2. For example, at $x \approx 0.01$ the average momentum transfer is $Q^2 \approx 1.6$ GeV^2. But at these low Q^2 it is not justifiable to consider only leading twist contributions to the structure function. The multiple scattering of strongly correlated $q\bar{q}$ pairs on the nuclear target now becomes important. This brings in the vector-meson contribution $F_2^{A,\mathrm{VM}}$ to the nuclear structure function (45). Its form is analogous to that of $F_2^{N,\mathrm{VM}}$ for the free nucleon [see Eq. (43)], where now the vector-meson-nucleon cross sections σ_{VN} are replaced

by corresponding nuclear cross sections σ_{VA}. The latter is related to the former via the Glauber- Gribov multiple scattering series [50,11]. Together with the scaling part $F_2^{A,\mathrm{as}}(x)$, which includes the nuclear interaction of uncorrelated $q\bar{q}$ pairs, we then calculate the full nuclear structure function $F_2^A(x,Q^2)$ according to Eq. (45).

In Fig. 7 we compare our results for $R(x,Q^2) = F_2^A(x,Q^2)/[AF_2^N(x,Q^2)]$, including vector mesons, with the data of the NMC collaboration [2]. For every x bin, $R(x,Q^2)$ is calculated using the corresponding average $\langle Q^2 \rangle$ as given in [2]. The result is shown by the solid line. We see that if one includes vector mesons the measured shadowing can be described quite well. As we already discussed in Eqs. (44) and (45), the contribution of uncorrelated quark pairs to F_2^N and F_2^A decreases with decreasing $Q^2 < Q_0^2 \approx 2$ GeV^2. Consequently, their contribution to the measured shadowing effect becomes smaller with decreasing $x(< 0.01)$ since there the experimental $\langle Q^2 \rangle$ falls off rapidly.

In summary we find that the scaling contribution to the nucleon structure function alone can account for only about half of the measured shadowing effect. The other half results from the interactions of strongly correlated $q\bar{q}$ pairs, i.e., vector mesons, with the target. The fact that the observed shadowing is only weakly Q^2 dependent [2] has now a plausible explanation: although the vector-meson contributions vanish at large Q^2 there is still a sizable shadowing effect due to the interaction of uncorrelated quarks or antiquarks with the nuclear target.

B. The large x region: Convolution model

In the region $x > 0.2$ nuclear structure functions are commonly described within the impulse approximation (see Fig. 8) ignoring final-state interaction of the nucleon debris with the remaining nuclear system.[3] The Feynman diagram in Fig. 8 is usually written in the form of a convolution (see, e.g., [32]):

$$F_2^A(x) = \int_x dy\, D_{N/A}(y)\, F_2^N(x/y). \qquad (50)$$

Here the structure function $F_2^N(x)$ is folded with the (light-cone) momentum distribution $D_{N/A}(y)$ of nucleons in the nucleus. Starting from the pioneer work [20] Eq. (50) has frequently been applied in calculations of Fermi motion and binding corrections [21–29]. The convolution formalism is also used to evaluate meson cloud effects [54], exchange currents corrections [25,55], etc. (for a review see Ref. [8]).

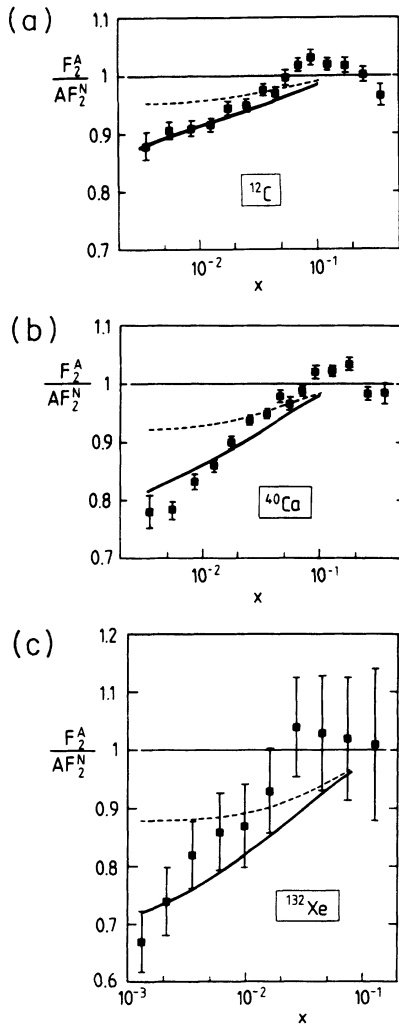However, as pointed out in a recent analysis [56], a derivation of the convolution model (50) even within

FIG. 7. The shadowing effect calculated for ^{12}C (a), ^{40}Ca (b), and ^{132}Xe (c) in comparison with the experimental data [2,3]. The dashed curve corresponds to large Q^2 ($Q^2 > 5$ GeV^2) and represents the scaling part of the nuclear shadowing. The solid curve is the result of the full calculation including the vector mesons. For every x bin we use averaged $\langle Q^2 \rangle$ given in [2].

---

[3]An attempt to estimate the influence of final-state interaction on leading twist nuclear structure functions was made in Refs. [51–53].
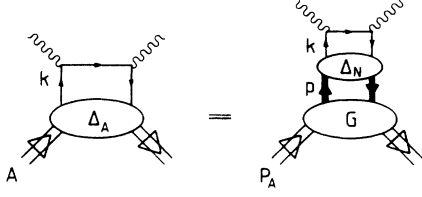
FIG. 8. Impulse approximation for the nuclear Compton amplitude.

the impulse approximation implies several assumptions which are generally not justified. In this section we re-examine the derivation of Eq. (50) on the basis of our covariant approach developed in Sec. II. It will turn out that off-shell effects are important, so that the simple convolution model is generally not a good approximation for F_2^A.

We start from Eq. (8) which gives the nuclear light-cone distribution function $f_A(x_A)$ in terms of the quark correlator $\Delta_A(k, P_A)$ in the nucleus. Consider now the diagram Fig. 8. It can be written as a convolution of the quark correlator $\widehat{\Delta}_N(k, p)$ in the bound nucleon and the nucleon propagator $G(p, P_A)$ in the nucleus:

$$\Delta_A(k, P_A) = -i \int \frac{d^4p}{(2\pi)^4} \, \mathrm{Tr}_N \left[\widehat{\Delta}_N(k, p) G(p, P_A) \right]. \quad (51)$$

Here and in the following the "hat" on $\widehat{\Delta}_N$ and other quantities indicates their matrix structure in nucleon Dirac space, and the trace Tr_N is taken with respect to nucleon variables. The four-momenta P_A, p, and k refer to the nucleus, the bound nucleon, and the quark in the nucleon, respectively. The quark propagator in the on-mass-shell nucleon (5) averaged over nucleon polarizations is related to $\widehat{\Delta}_N$ as follows:

$$\Delta_N(k, p) = \frac{1}{2} \mathrm{Tr}_N \left[\widehat{\Delta}_N(k, p)(\slashed{p} + M) \right]. \quad (52)$$

Substituting Eq. (51) into Eq. (8) we obtain for the nuclear light-cone distribution

$$f_A(x_A) = -i \int \frac{d^4p}{(2\pi)^4} \mathrm{Tr}_N \left[\widehat{f}_N(x', p^2) \, G(p, P_A) \right], \quad (53)$$

with $x_A = Q^2 / 2 P_A \cdot q$ and

$$\widehat{f}_N(x', p^2) = -i \int \frac{d^4k}{(2\pi)^4} \frac{\mathrm{Tr}_Q \left[\slashed{q} \, \widehat{\Delta}_N(k, p) \right]}{2p \cdot q} \delta \left(x' - \frac{k \cdot q}{p \cdot q} \right). \quad (54)$$

Here the trace Tr_Q is taken with respect to quark variables and $x' = Q^2 / 2p \cdot q$ is the Bjorken variable of an off-shell nucleon with four-momentum p.

Let us now examine the Lorentz structure of $\widehat{f}_N$ in the nucleon Dirac space. In general, it can be expanded in terms of a complete set of 16 Dirac matrices. However

there are only four independent terms[4] which can be constructed from the momenta p, q and the Dirac matrices:

$$\widehat{f}_N = f_S \, I + f_V^\mu \, \gamma_\mu + f_T^{\alpha\beta} \, \sigma_{\alpha\beta}, \quad (55)$$

with

$$f_S = \frac{f_0}{2M}, \quad (56a)$$

$$f_V^\mu = \frac{f_1}{2M^2} \, p^\mu + \frac{f_2}{2p \cdot q} \, q^\mu, \quad (56b)$$

$$f_T^{\alpha\beta} = \frac{f_3}{2p \cdot q \, M} \, p^\alpha q^\beta, \quad (56c)$$

where $\sigma_{\alpha\beta} = \frac{i}{2}[\gamma_\alpha, \gamma_\beta]$ and $f_i = f_i(x, p^2)$, $i = 0, 1, 2, 3$, are dimensionless Lorentz-invariant functions. The coefficients in Eq. (56) are chosen in such a way that the on-mass-shell distribution function averaged over the nucleon spin is given by

$$f_N(x) = \lim_{p^2 \to M^2} \frac{1}{2} \mathrm{Tr}[(\slashed{p} + M)\widehat{f}_N(x, p^2)] = f_0 + f_1 + f_2. \quad (57)$$

We see that the tensor term in (55) does not contribute to the unpolarized structure functions.

Substituting (55) into (53) one finds an equation which connects the nuclear light-cone distribution with the functions f_i:

$$f_A(x_A) = -i \int \frac{d^4p}{(2\pi)^4} \sum_{i=0}^{3} C_i(p, q) f_i(x', p^2). \quad (58)$$

The functions $C_i(p, q)$ are given by traces of the nucleon propagator G with the different Dirac matrices in Eq. (55):

$$C_0 = \frac{1}{2M} \, \mathrm{Tr} \, G(p, P_A), \quad (59a)$$

$$C_1 = \frac{1}{2M^2} \, \mathrm{Tr} \, [G(p, P_A)\slashed{p}], \quad (59b)$$

$$C_2 = \frac{1}{2p \cdot q} \mathrm{Tr} \, [G(p, P_A)\slashed{q}], \quad (59c)$$

$$C_3 = \frac{p^\alpha q^\beta}{2p \cdot q M} \, \mathrm{Tr} \, [G(p, P_A)\sigma_{\alpha\beta}]. \quad (59d)$$

We emphasize here that, in general, Eq. (58) does not reduce to the simple convolution formula (50) with respect to the light-cone momentum. There are two reasons for this. First, terms with different Lorentz structures in Eq. (55) are convoluted with correspondingly different nuclear distribution functions. Secondly, the structure functions in the off-shell region depend not only on the

---

[4]We ignore possible terms proportional to γ_5 and $\gamma_\alpha \gamma_5$ which do not contribute to the unpolarized structure functions.

scaling variable x' but also on the off-shell mass p^2 of the bound nucleon. This will now be examined in more detail.

In the following we shall consider the nuclear structure functions as functions of the "nucleon" Bjorken variable $x = Q^2/2Mq_0$ instead of the "nuclear" one, $x_A = Q^2/2M_A q_0$. The structure function F_2^A as a function x reads

$$F_2^A(x) = x\left[\mathcal{F}_A(x) - \mathcal{F}_A(-x)\right],\qquad(60)$$

$$\mathcal{F}_A(x) = \frac{M}{M_A} f_A\left(\frac{M}{M_A}x\right).\qquad(61)$$

One can easily see that the transformation (61) preserves the normalization of the nuclear distribution function as a function of x:

$$\int_{-M_A/M}^{M_A/M} dx\, \mathcal{F}_A(x) = \int_{-1}^{1} dx_A f_A(x_A) = 3A.\qquad(62)$$

Equation (58) can be simplified if one assumes that the nucleus is a nonrelativistic system. In this case, as shown in the Appendix, $\mathcal{A}_3$ vanishes up to terms of order $|\mathbf{p}|^3/M^3$ if one uses the nonrelativistic form for the nucleon propagator. Moreover, $\mathcal{A}_3 = 0$ for spinless nuclei. In the same approximation the functions $\mathcal{A}_0$, $\mathcal{A}_1$, and $\mathcal{A}_2$ are proportional to each other [see Eqs. (A7) in the Appendix]. This allows us to introduce one *unique* nucleon distribution function $D_{N/A}$ which, however, depends also on p^2. Using Eqs. (A7) in the Appendix we have,

$$\mathcal{F}_A(x) = \int_{y>|x|} \frac{dy}{y} \int dp^2\, D_{N/A}(y,p^2) f_N(x/y,p^2),\qquad(63)$$

$$\begin{aligned}f_N(x,p^2) &= \sqrt{p^2/M^2} f_0(x,p^2)\\ &\quad + (p^2/M^2) f_1(x,p^2) + f_2(x,p^2),\end{aligned}\qquad(64)$$

$$\begin{aligned}D_{N/A}(y,p^2) &= \int \frac{d^4p'}{(2\pi)^4} S(p')\left(1 + \frac{p_3'}{M}\right)\\ &\quad \times \delta\left(y - \frac{p_+'}{M}\right)\delta(p^2 - p'^2).\end{aligned}\qquad(65)$$

Equation (64) can be identified with the light-cone distribution function of the bound nucleon. In Eq. (65) we have introduced the nuclear spectral function

$$S(p) = 2\pi \sum_n \delta(p_0 - M - \varepsilon_n)|\Psi_n(\mathbf{p})|^2,\qquad(66)$$

where the sum includes all residual nuclear states with $A-1$ nucleons which carry together the momentum $-\mathbf{p}$. All other quantum numbers are denoted as n. The nucleon separation energy is defined as $\varepsilon_n = E_0(A) - E_n(A-1)$. Furthermore, $\Psi_n(\mathbf{p}) = \langle(A-1)_n, -\mathbf{p}|\Psi(0)|A\rangle$, where $\Psi(0)$ is the nonrelativistic nucleon field operator at $\mathbf{r} = 0$. The spectral function is normalized to the number of nucleons in the nucleus,

$$\int \frac{d^4p}{(2\pi)^4}\, S(p) = A,\qquad(67)$$

which guarantees the correct normalization of the nucleon distribution function in Eq. (65).

It is convenient to introduce also the distributions of quarks, $q(x,p^2)$, and antiquarks, $\bar{q}(x,p^2)$, in the bound nucleon. These are expressed through $f_N(x,p^2)$ by Eqs. (7):

$$q(x,p^2) = f_N(x,p^2),\qquad(68a)$$

$$\bar{q}(x,p^2) = -f_N(-x,p^2).\qquad(68b)$$

In terms of these distributions the structure functions of the bound nucleon are given by the usual parton-model formula [see Eq. (6)]. The relation between the nuclear and the bound-nucleon structure functions then reads:

$$F_2^A(x) = \int_x dy \int dp^2\, D_{N/A}(y,p^2) F_2^N(x/y;p^2).\qquad(69)$$

Let us examine this equation in more detail. The nucleon distribution (65) is strongly peaked around $p^2 = M^2$ and $y = 1$, with a characteristic width $\Delta y \sim p_F/M$, where p_F is the nucleon Fermi momentum. Expanding the bound-nucleon structure function in Eq. (63) in a Taylor series around these points and integrating term by term, one then obtains the following expression for the nuclear structure function per nucleon [57]:

$$\begin{aligned}F_2^A(x)/A &\simeq F_2^N(x) - \frac{\langle\varepsilon\rangle}{M} x F_2^{N\prime}(x) + \frac{\langle T\rangle}{3M} x^2 F_2^{N\prime\prime}(x)\\ &\quad + 2\frac{\langle\varepsilon\rangle - \langle T\rangle}{M}\left(p^2\frac{\partial F_2^N(x;p^2)}{\partial p^2}\right)_{p^2=M^2}.\end{aligned}\qquad(70)$$

Here $F_2^{N\prime}(x)$ and $F_2^{N\prime\prime}(x)$ are derivatives of the structure function with respect to x, and $\langle\varepsilon\rangle$ and $\langle T\rangle$ are the mean separation and kinetic energies of the bound nucleon,

$$\langle\varepsilon\rangle = \frac{1}{A}\int \frac{d^4p}{(2\pi)^4}\, S(p)\,\varepsilon,\qquad(71)$$

$$\langle T\rangle = \frac{1}{A}\int \frac{d^4p}{(2\pi)^4}\, S(p)\,\frac{\mathbf{p}^2}{2M}.\qquad(72)$$

Corrections to Eq. (70) are of higher order in $\langle\varepsilon\rangle/M$ and $\langle T\rangle/M$. One should also note that Eq. (70) can safely be used for $1 - x > p_F/M \sim 0.3$. In this region the condition $x/y \leq 1$ gives practically no restrictions on the integration over the nucleon momentum p in Eqs. (71) and (72).

The first three terms in Eq. (70) are identical to the result of [21,25] in their discussion of the EMC effect, while the last one reflects the leading contribution from the p^2 dependence of the bound-nucleon structure function. Let us first neglect the latter and discuss effects due to separation and kinetic energies. These terms are of opposite signs and the competition between them results in a behavior of the ratio $R(x) = F_2^A/AF_2^N$ at $x > 0.3$ similar to that seen in the experiment. As it was first pointed out in Ref. [21] and discussed by many authors (see, e.g., Ref. [8] for a review), this may account for the EMC effect at intermediate and large x. An important (and still open) problem in this respect is a reliable calculation of $\langle\varepsilon\rangle$ and $\langle T\rangle$ [27]. In a simple nuclear shell model the removal

energy is averaged over all occupied levels. One finds typical values $\langle \varepsilon \rangle \approx -(20\text{--}25)$ MeV and $\langle T \rangle \approx 18\text{--}20$ MeV. Correlations between nucleons change the simple mean-field picture significantly and lead to high momentum $(p > p_F)$ components in the nuclear spectral function (66). This in turn causes an increase of the average removal energy $\langle \varepsilon \rangle$. In order to demonstrate this let us consider the Koltun sum rule [58], which is exact if only two-body forces are present in the nuclear Hamiltonian:

$$\langle \varepsilon \rangle + \langle T \rangle = 2\mu_B. \tag{73}$$

Here $\mu_B \approx -8$ MeV is the nuclear binding energy per nucleon. In particular, Eq. (73) tells that an increase of $\langle T \rangle$ due to high momentum components implies also an increase of $|\langle \varepsilon \rangle|$. We refer in this respect to a recent calculation [59] of the spectral function of nuclear matter based on a variational method. This calculation shows that there is a significant probability to find nucleons with high momentum and large separation energies. Integration of the spectral function of Ref. [59] gives $\langle T \rangle \approx 38$ MeV and $\langle \varepsilon \rangle \approx -70$ MeV. In order to estimate these quantities for finite nuclei one usually assumes [28] that the high momentum component of the nucleon momentum distribution is about the same as in nuclear matter, which gives $\langle T \rangle \approx 35$ MeV for a wide range of nuclei. The latter quantity together with Eq. (73) leads to $\langle \varepsilon \rangle \approx -50$ MeV. It should be noted, however, that, even though a qualitative understanding of the EMC effect can be obtained using such values for $\langle \varepsilon \rangle$ and $\langle T \rangle$, a quantitative description is still lacking.

Let us finally discuss nuclear effects due to the off-mass-shell properties of nucleons bound in nuclei. We note in this respect that the analysis of Sec. II can be applied also to Eq. (54), which describes the quark and the antiquark distributions of the off-shell nucleon. We parametrize the loop momentum in Eq. (54) in terms of the Sudakov variables, $k = \alpha p + \beta q' + k_\perp$, where p is the nucleon momentum in Eq. (51) and $q' = q + x'p$. Assuming again that the quark correlator $\widehat{\Delta}_N$ is an analytic function of $s = (p - k)^2$, $u = (p + k)^2$, and k^2 we end up with equations similar to Eqs. (17) and (18), where, however, the squared nucleon mass M^2 is now replaced by p^2. In particular, for the quark distribution $q(x', p^2)$ we have

$$q(x', p^2) = \frac{1}{16\pi^2} \int ds \int_{-\infty}^{k_{\max}^2} dk^2 \, \rho_R(s, k^2, x', p^2), \tag{74}$$

where $k_{\max}^2 = x' \left[s/(x' - 1) + p^2 \right]$ [cf. Eq. (18)] and ρ_R is the quark spectral density given by an equation similar to Eq. (16).

We conclude from Eq. (74) that the p^2 dependence of the structure functions has two primary sources:

(1) Explicit dependence of the quark correlator $\widehat{\Delta}_N$ in Eq. (54) on p^2 ("dynamical" p^2 dependence). This leads to a p^2 dependence of parameters characterizing the quark spectral density ρ_R.

(2) Dependence of the invariant variables s and u on p^2 ("kinematical" p^2 dependence). This manifests

itself via the p^2 dependence of $k_{\max}^2$ in Eq. (74).

Taking both into account we obtain from Eq. (74),

$$\frac{\partial q(x, p^2)}{\partial p^2} = \frac{1}{16\pi^2} \int ds \left[x \, \rho_R(s, k_{\max}^2, x, p^2) \right.$$
$$\left. + \int_{-\infty}^{k_{\max}^2} dk^2 \, \frac{\partial \rho_R(s, k^2, x, p^2)}{\partial p^2} \right], \tag{75}$$

The first (positive) term in Eq. (75) arises from the p^2 dependence of $k_{\max}^2$. Its contribution to Eq. (70) leads to an enhancement of the nuclear binding effect. However, if only this "kinematical" p^2 dependence would be present the number of valence quarks in the nucleon would increase with p^2. Therefore, to fix the normalization of the valence quark distribution,

$$\frac{\partial}{\partial p^2} \int_0^1 dx \, [q(x, p^2) - \bar{q}(x, p^2)] = 0, \tag{76}$$

an explicit p^2 dependence of the quark spectral density is necessary. [Of course, cancelation of the "kinematical" and the "dynamical" p^2 dependences in the integral (76) does not imply that $\partial q/\partial p^2$ vanishes for a given value of x.]

Let us now evaluate this effect using the model developed in Sec. III. We consider the region of large $x > 0.2$ where one can neglect the sea part of the quark distributions. Therefore we keep contributions to the quark spectral density ρ_R only from mechanism (i) which dominates in the large x region. Recalling Eq. (22) we now have

$$\rho_R(s, k^2, x, p^2) = \Phi(k^2, p^2)\delta(s - \bar{s}). \tag{77}$$

We assume that the k^2 dependence of the function $\Phi(k^2, p^2)$ is the same as for the on-mass-shell nucleon, Eq. (36), and that the p^2 dependence comes from the corresponding dependence of the cutoff parameter Λ_V, $\Phi(k^2, p^2) = \Phi(k^2; \Lambda_V(p^2))$. We fix the p^2 dependence of Λ_V in such a way that Eq. (76) is satisfied. Solving this equation we find $\partial \Lambda_V^2/\partial p^2 \approx 0.15$ at $p^2 = M^2$.
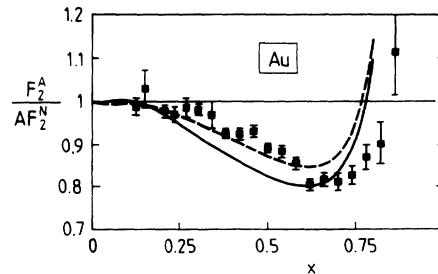

FIG. 9. The ratio of the nuclear and nucleon structure functions calculated using Eq. (70) with $\langle \varepsilon \rangle = -50$ MeV and $\langle T \rangle = 20$ MeV. The dashed curve is the result without corrections due to the p^2 dependence of the bound-nucleon structure function. The solid line is the result of the full calculation. The experimental data for ^{197}Au are taken from [7].
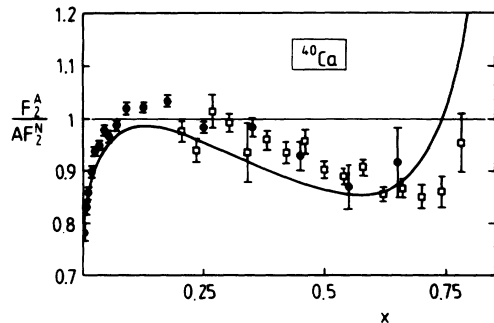
FIG. 10. Result of the full calculation for ^{40}Ca, including shadowing, binding, and off-shell effects.

The p^2 dependence of Λ_V can be viewed as an effect of changing the bound nucleon size $R_N \sim 1/\Lambda_V$ in nuclei. In fact, $\partial \Lambda_V^2/\partial p^2 > 0$ implies a "swelling" of the nucleon in the nuclear environment. For the relative change of the radius of the bound nucleon, we obtain

$$\frac{\delta R_N}{R_N} \sim -\frac{1}{2}\frac{\delta \Lambda_V^2}{\Lambda_V^2} = -\frac{\partial \Lambda_V^2}{\partial p^2}\frac{M\langle \varepsilon - T\rangle}{\Lambda_V^2}. \qquad (78)$$

In this way we find a very small (0.8%) increase of the size of a nucleon bound in the nucleus, indicating a remarkable stability of the nucleon.[5] This result is compatible with recent findings using quite a different approach [53].

In Fig. 9 we show a typical result for $R(x) = F_2^A(x)/AF_2^N(x)$ calculated using Eq. (70). The dashed curve corresponds to the impulse approximation neglecting any p^2 dependence. The solid curve is the result of the full calculation including Eq. (75). The "kinematical" and the "dynamical" p^2 dependence tend to cancel each other partly at small $x < 0.3$. At $x \sim 0.5$–0.6 the effect of the p^2 dependence of the bound-nucleon structure function is clearly visible and leads to an enhancement of the nuclear binding effect.

For $x > 0.7$ one should keep in mind that Eq. (70) cannot be applied in this region. Instead, one should use Eq. (69) to which Eq. (70) is an approximation. Also, the ratio F_2^A/AF_2^N becomes sensitive to uncertainties in the shape and magnitude of the free-nucleon structure function at large x.

A result (for ^{40}Ca) of the unified description which incorporates both the shadowing effect at small x and the binding, Fermi motion, and off-shell corrections at large x is shown in Fig. 10. While the overall pattern of the data is quite well reproduced, we see that once the off-shell p^2 dependence of the bound-nucleon structure function is included, there is some room for a possible

small enhancement of F_2^A due to nuclear pion cloud effects [25,55] for $0.2 < x < 0.4$, which are omitted in the present calculations.

V. SUMMARY AND CONCLUSIONS

We have presented a unified description of deep-inelastic scattering on nuclear targets which covers the whole region $10^{-3} < x \lesssim 1$ of the Bjorken variable. Our starting point is a relativistic, covariant formalism which makes use of the analytic properties of quark correlators. In the infinite momentum frame we recover the usual parton model. In the laboratory system, which is the appropriate frame in which to investigate nuclear structure functions, this approach naturally incorporates two basic mechanisms, namely, (i) scattering from quarks and antiquarks in the target and (ii) photon conversion into a quark-antiquark pair and subsequent interactions of this pair with target constituents.

For small x, say, below $x < 0.1$, the second one of these processes dominates and produces shadowing. At the momentum transfers, Q^2, typical of the current experiments we find that only about half of the observed shadowing comes from the coherent interaction of uncorrelated $q\bar{q}$ pairs with target nucleons, the mechanism discussed in Ref. [16]. The other half comes from the coherent scattering of strongly correlated pairs, i.e., vector mesons.

At larger values of the Bjorken variable $(x > 0.2)$, scattering from the quarks of a single bound nucleon dominates. The leading nuclear effects are now binding and Fermi motion, as pointed out already in previous studies. However, we find that the naive convolution formalism needs to be generalized to incorporate off-shell effects characteristic of bound nucleons. These off-shell effects are by no means small. They reduce $F_2^A(x)/A$ with respect to the free-nucleon structure function $F_2^N(x)$ and effectively enhance the binding correction.

ACKNOWLEDGMENTS

APPENDIX: NONRELATIVISTIC REDUCTION OF MATRIX ELEMENTS

Consider Eq. (58) written for the distribution function $\mathcal{F}_A(x)$. For the following it is convenient to multiply it by x. We have

$$x\mathcal{F}_A(x) = -i\int \frac{d^4p}{(2\pi)^4}\sum_{i=0}^{3}\mathcal{A}_i\, x'f_i(x',p^2), \qquad (A1)$$

---

[5]In Ref. [31] the EMC effect is attributed to a 10% increase of the nucleon radius in the nucleus. We emphasize here that in our study of nuclear binding and off-shell effects this increase of size is reduced by an order of magnitude.

where

$$\mathcal{A}_0 = \frac{p_+}{M} \operatorname{Tr} \bar{G}(p), \tag{A2a}$$

$$\mathcal{A}_1 = \frac{p_+}{M^2} \operatorname{Tr}[\bar{G}(p)\not{p}], \tag{A2b}$$

$$\mathcal{A}_2 = \operatorname{Tr}[\bar{G}(p)\gamma_+], \tag{A2c}$$

$$\mathcal{A}_3 = \frac{p^\alpha q^\beta}{M q_0} \operatorname{Tr}\left[\bar{G}(p)\sigma_{\alpha\beta}\right]. \tag{A2d}$$

Equations (A2) are written in the laboratory frame where $P_A = (M_A, 0)$, $q = (q_0, 0_T, -|\mathbf{q}|)$, $p_+ = p_0 + p_3$, and $\gamma_+ = \gamma_0 + \gamma_3$. We have used the fact that $x/x' = p_+/M$. Also we have introduced $\bar{G}(p) = G(p, P_A)/2M_A$, where the factor $2M_A$ ensures that $\bar{G}$ is independent of the normalization of the nuclear state.

Consider a nonrelativistic reduction of matrix elements (A2). We start from the nucleon propagator which can be written as follows:

$$\bar{G}(p) = -i \int dt\, e^{ip_0 t} \langle T\left[N(\mathbf{p},t)\bar{N}(\mathbf{p},0)\right]\rangle, \tag{A3}$$

where $N(\mathbf{p},t) = \int d^3\mathbf{r}\, \exp(-i\mathbf{p}\cdot\mathbf{r})\, N(\mathbf{r},t)$ is the nucleon field operator in a mixed $(\mathbf{p},t)$ representation and the brackets denote the averaging over the nuclear ground state, $\langle\cdots\rangle = \langle A|\cdots|A\rangle/\langle A|A\rangle$ (see also Sec. II).

We apply a $1/c$-expansion technique to obtain an approximate solution of the Dirac equation for the nucleon field N in the nonrelativistic limit $|\mathbf{p}|/M \to 0$. Up to terms of order $1/c^3$ the nucleon field N can be written as follows:

$$N(\mathbf{p},t) = C\left(\begin{array}{c}\Psi(\mathbf{p},t) \\ \frac{\mathbf{p}\cdot\boldsymbol{\sigma}}{2M}\Psi(\mathbf{p},t)\end{array}\right). \tag{A4}$$

We have introduced a two-component nonrelativistic nucleon field Ψ. The normalization constant C is fixed by

the charge (particle number) conservation condition,

$$\int d^3\mathbf{r}\, N^\dagger(\mathbf{r})N(\mathbf{r}) = \int d^3\mathbf{r}\, \Psi^\dagger(\mathbf{r})\Psi(\mathbf{r}), \tag{A5}$$

which gives $C = 1 - \mathbf{p}^2/8M^2$.

Now we are prepared to calculate traces (A2). We write the nucleon four-momentum as $p = (M + \varepsilon, \mathbf{p})$. The squared four-momentum is $p^2 \simeq M^2 + 2M(\varepsilon - T)$, where $T = \mathbf{p}^2/2M$ is the nonrelativistic kinetic energy. We also introduce the nonrelativistic nucleon propagator

$$\mathcal{G}(p) = -i \int dt\, e^{ip_0 t} \langle T\left[\Psi(\mathbf{p},t)\Psi^\dagger(\mathbf{p},0)\right]\rangle. \tag{A6}$$

Using Eqs. (A4) and (A6) we have

$$\mathcal{A}_0(p) = \sqrt{\frac{p^2}{M^2}}\left(1 + \frac{p_3}{M}\right)\operatorname{tr}\mathcal{G}(p), \tag{A7a}$$

$$\mathcal{A}_1(p) = \frac{p^2}{M^2}\left(1 + \frac{p_3}{M}\right)\operatorname{tr}\mathcal{G}(p), \tag{A7b}$$

$$\mathcal{A}_2(p) = \left(1 + \frac{p_3}{M}\right)\operatorname{tr}\mathcal{G}(p), \tag{A7c}$$

$$\mathcal{A}_3(p) = i\frac{2\varepsilon - T}{2M^2}\operatorname{tr}\left[\mathcal{G}(p)\,(\mathbf{p}\times\boldsymbol{\sigma})_3\right], \tag{A7d}$$

where the trace is taken with respect to spin. Corrections to Eqs. (A7) are of order $1/c^3$. From the last equation we see that $\mathcal{A}_3$ appears only in the order $|\mathbf{p}|^3/M^3$ and can therefore be neglected at the present level of accuracy. Moreover, this term vanishes identically for spinless nuclei, where $\operatorname{tr}\mathcal{G}\boldsymbol{\sigma} = 0$. Substituting Eqs. (A7) into Eq. (A1) and closing the integration contour in the upper half of the complex p_0 plane we arrive at Eq. (63).

[1] NM Collaboration, P. Amaudruz et al., Z. Phys. C 53, 73 (1992).
[2] NM Collaboration, P. Amaudruz et al., Z. Phys. C 51, 387 (1991).
[3] FNAL E665, M. R. Adams et al., Phys. Rev. Lett. 68, 3266 (1992).
[4] EM Collaboration, J. Ashman et al., Phys. Lett. B 202, 603 (1988).
[5] BCDMS Collaboration, A. C. Benvenuti et al., Phys. Lett. B 189, 483 (1987).
[6] SLAC E140, S. Dasu et al., Phys. Rev. Lett. 60, 2591 (1988).
[7] SLAC E139, R. G. Arnold et al., Phys. Rev. Lett. 52, 727 (1984).
[8] R. G. Bickerstaff and A. W. Thomas, J. Phys. G 15, 1523 (1989).
[9] R. J. M. Covolan and E. Predazzi, in Hadronic Physics With Multi-GeV Electrons, Les Houches, 1990, edited by B. Desplanques and D. Goutte (Nova Science Publishers, New York, 1990).
[10] M. Arneodo, Report No. CERN-PPE/92-113, 1992.
[11] G. Piller and W. Weise, Phys. Rev. C 42, R1834 (1990).
[12] C. L. Bilchak, D. Schildknecht, and J. D. Stroughair, Phys. Lett. B 214, 441 (1988).
[13] G. Shaw, Phys. Lett. B 228, 125 (1989).
[14] V. D. Duca, S. J. Brodsky, and P. Hoyer, Phys. Rev. D 46, 931 (1992).
[15] L. L. Frankfurt and M. I. Strikman, Nucl. Phys. B316, 340 (1989).
[16] S. J. Brodsky and H. J. Lu, Phys. Rev. Lett. 64, 1342 (1990).
[17] N. N. Nikolaev and B. G. Zakharov, Z. Phys. C 49, 607 (1991).
[18] B. Badełek and J. Kwieciński, Nucl. Phys. B370, 278 (1992).
[19] W. Melnitchouk and A. W. Thomas, Phys. Lett. B 317, 437 (1993).
[20] G. B. West, Phys. Lett. 37B, 509 (1971).
[21] S. V. Akulinichev, S. A. Kulagin, and G. M. Vagradov, Phys. Lett. 158B, 485 (1985).
[22] S. V. Akulinichev, S. Shlomo, S. A. Kulagin, and G. M. Vagradov, Phys. Rev. Lett. 55, 2239 (1985).
[23] B. L. Birbrair, E. M. Levin, and A. G. Shuvaev, Nucl. Phys. A491, 618 (1989).
[24] G. V. Dunne and A. W. Thomas, Nucl. Phys. A455, 701 (1986).

[25] S. A. Kulagin, Nucl. Phys. **A500**, 653 (1989).

[26] H. Jung and G. A. Miller, Phys. Lett. B **200**, 351 (1988).

[27] S. Shlomo and G. M. Vagradov, Phys. Lett. B **232**, 19 (1989).

[28] C. Ciofi degli Atti and S. Liuti, Phys. Lett. B **225**, 215 (1989).

[29] A. E. L. Dieperink and G. A. Miller, Phys. Rev. C **44**, 866 (1991).

[30] F. Gross and S. Liuti, Phys. Rev. C **45**, 1374 (1992).

[31] V. Barone et al., Z. Phys. C **58**, 541 (1993).

[32] R. L. Jaffe, in *Relativistic Dynamics and Quark-Nuclear Physics*, edited by M. B. Johnson and A. Pickleseimer (Wiley, New York, 1985).

[33] B. L. Ioffe, V. A. Khoze, and L. N. Lipatov, *Hard Processes: Phenomenology, Quark-Parton Model* (Elsevier Science Publishers, North Holland, 1984).

[34] G. B. West, Phys. Rev. Lett. **24**, 1206 (1970).

[35] P. V. Landshoff, J. C. Polkinghorne, and R. D. Short, Nucl. Phys. **B28**, 225 (1971).

[36] P. D. B. Collins, *Regge Theory and High-Energy Physics* (Cambridge University Press, Cambridge, 1977).

[37] A. Donnachie and P. V. Landshoff, Phys. Lett. B **296**, 227 (1992).

[38] V. A. Matveev, R. M. Muradyan, and A. N. Tavkhelidze, Nuovo Cimento Lett. **7**, 719 (1973).

[39] S. J. Brodsky and G. R. Farrar, Phys. Rev. Lett. **31**, 1153 (1973).

[40] NM Collaboration, P. Amaudruz et al., Phys. Lett. B **295**, 159 (1992).

[41] T. S. Mattison et al., Phys. Rev. D **42**, 1311 (1990).

[42] CDHSW Collaboration, P. Berge et al., Z. Phys. C **49**, 187 (1991).

[43] A. W. Schreiber, A. I. Signal, and A. W. Thomas, Phys.

[44] Particle Data Group, K. Hikasa et al., Phys. Rev. D **45**, S1 (1992).

Rev. D **44**, 2653 (1991).

[45] R. F. Schwitters and K. Strauch, Annu. Rev. Nucl. Part. Sci. **26**, 89 (1976).

[46] T. H. Bauer, R. D. Spital, D. R. Yennie, and F. M. Pipkin, Rev. Mod. Phys. **50**, 261 (1978).

[47] B. Badełek and J. Kwieciński, Phys. Lett. B **295**, 263 (1992).

[48] R. J. Glauber, in *Lectures in Theoretical Physics*, edited by W. E. Brittin et al. (Interscience, New York, 1959).

[49] V. Franco, Phys. Rev. C **24**, 748 (1972).

[50] V. N. Gribov, Zh. Eksp. Teor. Fiz. **57**, 1306 (1969) [Sov. Phys. JETP **30**, 709 (1970)].

[51] A. W. Thomas, A. Michels, A. W. Schreiber, and P. A. M. Guichon, Phys. Lett. B **233**, 43 (1989).

[52] S. A. Kulagin, in *Quarks '90*, edited by V. A. Matveev et al. (World Scientific, Singapore, 1991).

[53] K. Saito and A. W. Thomas, "A microscopic understanding of the structure functions of finite nuclei," Report No. ADP-93-220/T138, 1993.

[54] P. J. Mulders, A. W. Schreiber, and H. Meyer, Nucl. Phys. **A549**, 498 (1992).

[55] M. Ericson and A. W. Thomas, Phys. Lett. **128B**, 112 (1983).

[56] W. Melnitchouk, A. W. Schreiber, and A. W. Thomas, Phys. Rev. D **49**, 1183 (1994).

[57] S. A. Kulagin, G. Piller, and W. Weise, in *Quarks '92*, edited by D. Grigoriev et al. (World Scientific, Singapore, 1991).

[58] D. S. Koltun, Phys. Rev. Lett. **28**, 182 (1972).

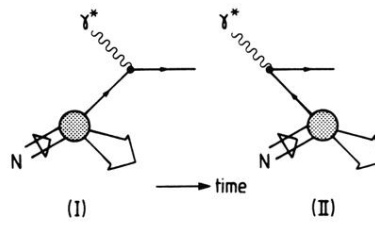[59] O. Benhar, A. Fabrocini, and S. Fantoni, Nucl. Phys. **A505**, 267 (1989).
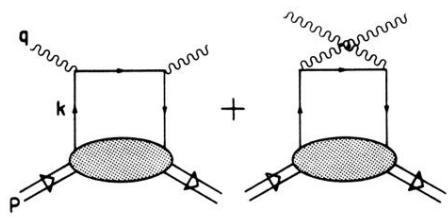
FIG. 1. Two basic mechanisms of deep-inelastic scattering.

FIG. 2. Compton amplitude to the leading order in Q^2.